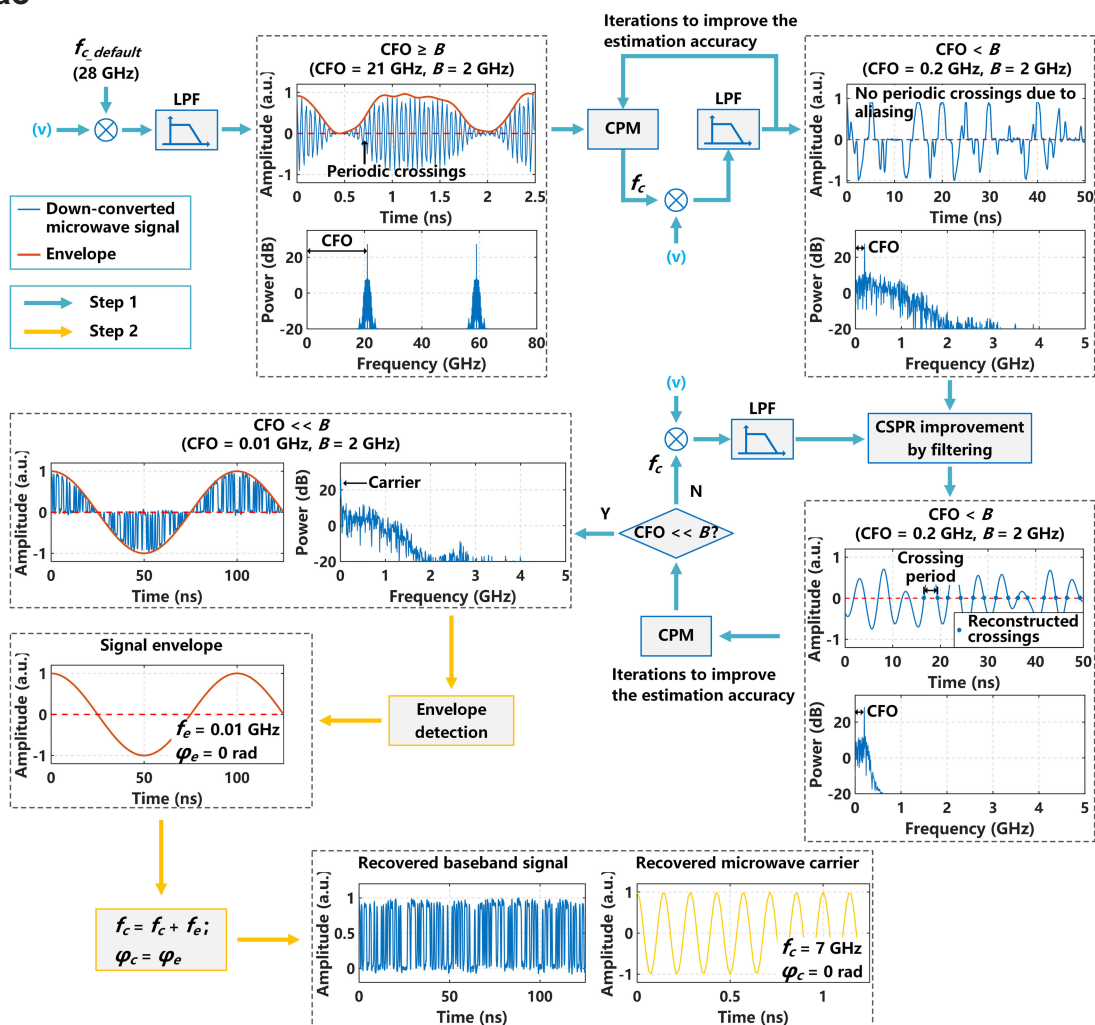


# An Approach to Wideband and High Accuracy Microwave Photonic Signal Carrier Recovery Based on Carrier Period Measurement

Volume 11, Number 4, August 2019

Qingming Zhu  
Ruiyuan Cao  
Shaohua An  
Yikai Su  
Jianping Yao



# An Approach to Wideband and High Accuracy Microwave Photonic Signal Carrier Recovery Based on Carrier Period Measurement

Qingming Zhu <sup>1</sup>, Ruiyuan Cao,<sup>1</sup> Shaohua An <sup>1</sup>, Yikai Su <sup>1</sup>,  
and Jianping Yao <sup>2</sup>

<sup>1</sup>State Key Laboratory of Advanced Optical Communication Systems and Networks,  
Department of Electronic Engineering, Shanghai Jiao Tong University, Shanghai  
200240, China

<sup>2</sup>Microwave Photonics Research Laboratory, School of Electrical Engineering and  
Computer Science, University of Ottawa, Ottawa, ON K1N 6N5, Canada

DOI:10.1109/JPHOT.2019.2929218

This work is licensed under a Creative Commons Attribution 4.0 License. For more information, see  
<https://creativecommons.org/licenses/by/4.0/>

Manuscript received June 10, 2019; revised July 4, 2019; accepted July 11, 2019. Date of publication July 24, 2019; date of current version July 30, 2019. This work was supported in part by the National Natural Science Foundation of China under Grant 61835008/61860206001, and in part by the Science and Technology Commission of Shanghai Municipality under Grant 16XD1401400/17500710900. Corresponding author: Yikai Su (e-mail: yikaisu@sjtu.edu.cn)

**Abstract:** We propose and experimentally demonstrate an approach to carrier frequency and phase recovery of a microwave photonic signal based on carrier period measurement (CPM). In the approach, a coarse carrier frequency offset (CFO) estimation is first performed, which is realized by measuring the crossing period of the microwave signal with its mean level. Then, an envelope detection method is used to simultaneously estimate the residual CFO and the carrier phase. Through the two steps, wideband and high-accuracy carrier recovery can be realized. The proposed approach is validated by an experiment. Effective carrier recovery of a microwave photonic signal is achieved with a carrier frequency varying from 7 to 37 GHz carrying a 2-Gbaud ON-OFF-keying or quadrature phase shift keying baseband signal. The CFO estimation range is from  $-21$  to  $+9$  GHz, and the CFO estimation errors are less than 0.1 MHz.

**Index Terms:** Carrier recovery, carrier period measurement, microwave photonics, digital signal processing.

## 1. Introduction

Microwave photonics has been extensively studied and found wide applications in microwave and optical systems [1], [2]. Among the numerous photonics-assisted microwave generation methods [2]–[6], optical heterodyne detection [3], [4] is a solution that exhibits low complexity and high capability in generating an ultra-high-frequency microwave signal, with its frequency determined by the wavelength spacing between two optical waves. For such a generation method using two free running laser sources, an important issue is the random carrier frequency offset (CFO) and phase noise in the generated microwave signal, which will deteriorate the performance of a microwave system using the generated microwave source. To precisely recover the baseband data, an approach to accurately recover the microwave carrier frequency and phase is highly needed.

Some carrier recovery methods have been proposed and demonstrated in microwave photonic systems, including  $M$ -th power algorithms [7]–[10], phase-locked loops (PLLs) [2], [10]–[12], RF-pilot aided algorithms [12]–[15], and others [16]–[20]. In an  $M$ -th power algorithm, CFO estimation is performed by applying nonlinear power operations to a microwave signal to estimate its carrier. The major limitation of the approach is that it is modulation format dependent [21], and the CFO estimation range is limited to  $\pm R_s/M$  [22], where  $R_s$  is the symbol rate. A phase-locked loop (PLL) can be employed to track the carrier phase that is slowly varying. A commercially available laser source, however, usually exhibits a wide linewidth and correspondingly a fast-changing phase noise [2], [23], which requires the PLL to have an ultra-short loop. An RF-pilot aided algorithm employs a narrow-band filter to extract the microwave carrier, while the CFO estimation range is limited to the filter bandwidth [24], [25]. Therefore, the applications of these methods [2], [7]–[20] may be limited by the relatively small CFO estimation range. A wideband carrier recovery method can recover different microwave frequencies through the same implementation; it is a general solution to carrier frequency recovery problems and may be desired in various microwave photonic systems operating at different microwave frequencies. However, no approach to carrier frequency and phase recovery of a microwave photonic signal with a wide CFO range ( $\pm 5$  GHz or beyond) has been demonstrated. There are also some carrier recovery methods adopted in wireless systems and coherent optical systems, such as blind frequency search (BFS) algorithms [21], [26]–[28], FFT-based algorithms [22], [24], [29], training sequence-based algorithms [30]–[34], and so forth [35]–[37]. The BFS and FFT-based algorithms may achieve a large CFO estimation range of  $\pm F_s/2$ , but their computational complexities are typically high due to the large iteration number and the large-size FFT operation, respectively. The training sequence-based algorithms can realize carrier frequency and phase recovery with low computational complexities and do not depend on the modulation formats. However, their CFO estimation ranges are limited to  $\pm R_s/2$ , and the training symbols contribute to the data rate overheads. A detailed comparison of the existing carrier recovery methods will be provided in Section 3.

In this paper, we propose and experimentally demonstrate an approach to implement carrier frequency and phase recovery of a microwave photonic signal with a wide CFO estimation range up to 30 GHz. The basic idea of the approach is to reconstruct the microwave carrier through the periodic carrier waveform from a received microwave signal. The approach is implemented in two steps. In the first step, coarse CFO estimation is carried out. Then, fine CFO estimation and phase estimation are performed in the second step. To realize the coarse CFO estimation, we use a carrier period measurement (CPM) method to obtain the crossing period  $T_c$  of a microwave signal with its mean level. The CFO is then estimated to be  $1/(2T_c)$ . Since  $T_c$  is  $\geq 1/F_s$ , where  $F_s$  is the sampling frequency of the digital signal, it is possible to achieve a wide CFO estimation range up to  $F_s/2$ . Note that the CPM method can only estimate the CFO magnitude. To obtain the sign of the CFO, a CFO sign recognition operation reported in [21] is also employed in the proposed approach. After the coarse CFO estimation, an envelope detection method based on fitting is used to simultaneously estimate the residual CFO and the carrier phase. Furthermore, to reduce the computational complexity, down-sampling operations reported in [21] are adopted during the two recovery steps. Although the carrier recovery approach is proposed for heterodyne detection systems, it can also be used in homodyne detection systems such as coherent optical systems, which will be discussed in Section 3. The feasibility of the approach is experimentally validated, in which carrier recovery of a microwave photonic signal is performed having a carrier frequency varied from 7 GHz to 37 GHz for two different modulation formats of on-off-keying (OOK) and quadrature phase shift keying (QPSK) with a baud rate of 2 Gbaud. Note that, since the proposed approach is based on the periodicity measurement of the microwave carrier, it can be used for any modulation format of the baseband signal, e.g., orthogonal frequency division multiplexing (OFDM) or quadrature amplitude modulation (QAM). Similarly, the performance of the proposed approach is independent of the baud rate of the baseband signal in theory. After optical-to-electrical conversion, the microwave signal is received by a software-defined radio receiver [38], [39]. This receiver is implemented by a high-speed analog-to-digital converter (ADC) and a digital signal

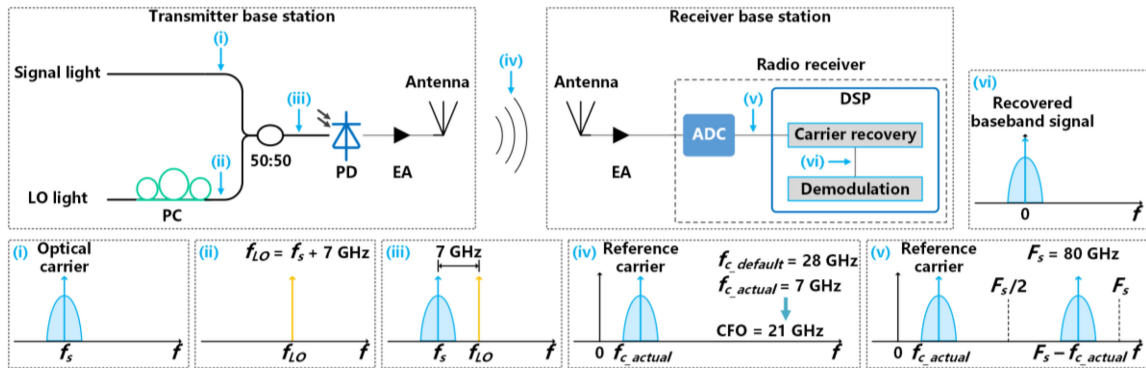


Fig. 1. A microwave generation and detection system architecture based on optical heterodyne detection. Insets (i)–(vi) show the frequency spectra of the optical/microwave signals. As an example, the frequency spacing between the signal light and the LO light is 7 GHz, and the default microwave carrier frequency is 28 GHz. The CFO is therefore 21 GHz, and a carrier recovery process is required. LO: local oscillator. PC: polarization controller. PD: photodetector. EA: electrical amplifier. ADC: analog-to-digital converter. DSP: digital signal processor.  $f_s$ : carrier frequency of the signal light.  $f_{LO}$ : carrier frequency of the LO light.  $f_{c\_default}$ : default carrier frequency.  $f_{c\_actual}$ : actual carrier frequency.  $F_s$ : sampling frequency.

processor (DSP). The bandwidth of the ADC is sufficient to sample the microwave signal, thus avoiding other high-speed electronic devices including a microwave source, a mixer and a power amplifier. In practical applications, the software-defined radio receiver may be desired for the low system complexity and high flexibility [38] if high-sampling-rate ADCs are commercially available. For the received microwave signal carrying the OOK or QPSK data, the proposed approach allows a CFO estimation range from  $-21$  GHz to  $+9$  GHz, with respect to a default carrier frequency of 28 GHz. Note that the upper bound of the estimation range is limited to  $\sim 38$  GHz due to the limited sampling rate of the ADC. The lower bound is related to the maximal cut-off frequency of a low-pass filter (LPF) employed after digital down-conversion, which is 20 GHz. In all the measurements, the CFO estimation errors are less than 0.1 MHz if the frame duration of the received signal is 10  $\mu$ s.

## 2. System Architecture and Algorithm Design

Fig. 1 shows a general microwave generation and detection system architecture, in which the proposed carrier recovery approach can be used. This architecture is commonly employed in fiber-wireless-integration (FWI) systems [40] and some radio-over-fiber (RoF) systems [9]. At the transmitter base station, a signal light carrying baseband data is received. A local oscillator (LO) light is provided with certain frequency spacing from the signal light. The carrier frequencies of the signal light and the LO light are denoted by  $f_s$  and  $f_{LO}$ , respectively. The two lights are combined by a 3-dB coupler and then fed into a photodetector for optical heterodyne detection. The detected signal consists of a baseband component and a microwave component, and only the microwave component can be delivered over a wireless link by antennas. The actual microwave carrier frequency  $f_{c\_actual}$  is unknown and may be significantly different from the default carrier frequency  $f_{c\_default}$ , therefore carrier recovery is needed. At the receiver base station, the received microwave signal is amplified and sent to a software-defined radio receiver for detection. The receiver comprises of a high-speed ADC and a DSP. Using the carrier recovery approach implemented in the DSP, the alternating current (AC) coupled microwave signal is down-converted to a direct current (DC) coupled baseband signal. It is worth noting that, to ease the implementation of this approach, a reference carrier is required to increase the carrier-to-signal power ratio (CSPR) of the microwave signal, which can be generated by beating the optical carrier of the signal light with the LO light in the photodetector. This means that the optical carrier of the signal light needs to be preserved in electrical-to-optical conversion. Although the proposed approach is implemented in a software-defined radio receiver, it

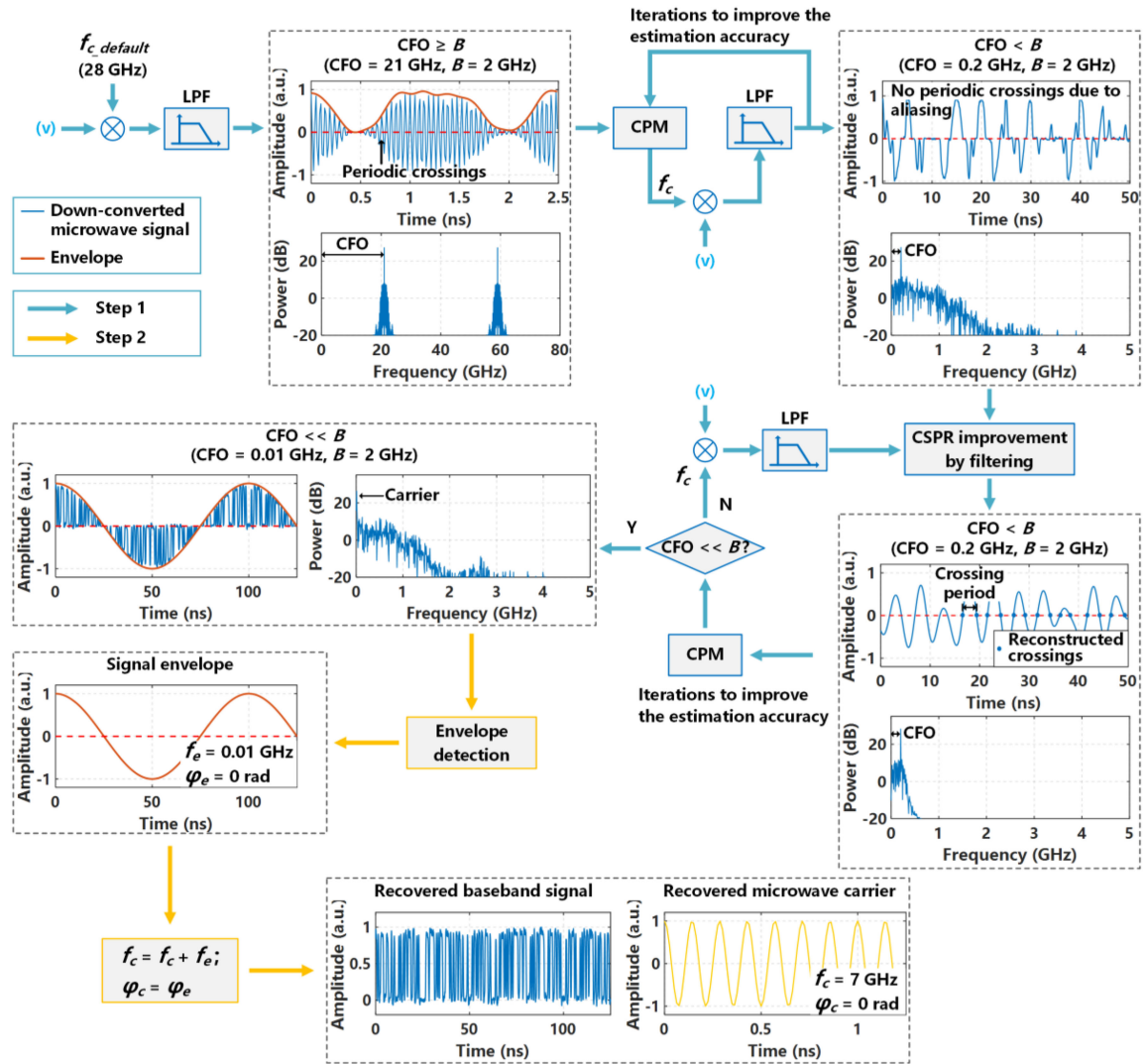


Fig. 2. An example of the carrier recovery process. LPF: low-pass filter.  $B$ : bandwidth of the baseband signal.  $f_c$ : estimated carrier frequency.  $\varphi_c$ : estimated carrier phase.  $f_e$ : frequency of the detected envelope.  $\varphi_e$ : phase of the detected envelope.

is possible to use the approach in an analog radio receiver, where a down-converter is placed before the ADC to relax the bandwidth requirement of the ADC. A discussion of the system applications of this approach will be included in Section 3.

To illustrate the operation principle of the proposed approach, an example of the carrier recovery process is shown in Fig. 2. The approach comprises of two steps for coarse recovery and fine recovery. The received microwave signal is assumed to carry binary data. The electrical bandwidth of the baseband signal is denoted by  $B$ . The initial CFO of the microwave signal is assumed to be  $\geq B$ . In step 1, the microwave signal is firstly down-converted by mixing it with the default microwave carrier at  $f_{c, default}$ . In this example, the initial CFO = 21 GHz,  $B = 2$  GHz, and  $F_s = 80$  GHz. The down-converted signal waveform shows periodic crossings with its mean level during the transmission of consecutive "1" bits. Thus, the initial CFO can be estimated by a CPM method, which searches for two adjacent crossing points in the signal waveform and calculates their time difference. The time

difference is considered as the crossing period and denoted as  $T_c$ . The estimated CFO is then given by  $1/(2T_c)$ , e.g., the initial CFO is estimated to be 19.7 GHz. The estimated carrier frequency  $f_c$  is updated accordingly, and down-conversion of the received microwave signal is performed again. However, the CFO estimation error in a single CPM process (e.g.,  $19.7 - 21 = -1.3$  GHz) is relatively large due to the limited time resolution of  $1/F_s$ , especially if the CFO approaches  $F_s/2$  so that  $T_c$  approaches  $1/F_s$ . To improve the estimation accuracy while maintaining the same estimation range, multiple iterations of the CPM process are required. When the CFO decreases to less than  $B$  (e.g., 0.2 GHz), aliasing occurs at baseband frequencies so that the periodic crossing points disappear. To ensure effective carrier recovery, the CSPR of the microwave signal needs to be higher than certain level to alleviate the interference of the carried data, and it is related to the CSPR of the modulated signal light and the performance of a digital LPF. The filter bandwidth is less than  $B$ . The periodic crossings are reconstructed in the filtered signal, enabling the following CPM iterations. After step 1, the CFO decreases to several orders of magnitude less than  $B$ , e.g., CFO is 0.01 GHz. In such case, the signal envelope is the down-converted microwave carrier. An envelope detection process is then carried out to estimate both the residual CFO and the carrier phase. The frequency of the detected envelope is the residual CFO, and its phase is equal to the carrier phase. In this example, the frequency and phase of the recovered microwave carrier is 7 GHz and 0 rad, respectively. Afterwards, the frequency offset of the recovered baseband signal is well below  $1/T_{frame}$ , where  $T_{frame}$  is the frame duration, hence it is negligible for the demodulation of the received frame. Note that this work mainly focuses on the wideband and high accuracy carrier frequency estimation, and the carrier phase is estimated as a constant. Therefore, the phase estimation scheme works with the lasers having narrow linewidths, e.g., several kilohertz. Note that, low phase noise is usually a basic requirement in practical microwave systems. For example, the phase noise requirement in the long-term evolution (LTE) network is  $\leq 94$  dBc/Hz at 10 KHz [41], [42]. To achieve this through optical heterodyne beating, the two lasers are typically required to possess sub-KHz linewidths [42], [43]. Therefore, the proposed carrier recovery method with linewidth tolerance of several kilohertz can compensate the phase noise in practical microwave systems. Also, a possibility of improving the linewidth tolerance is to combine the proposed carrier recovery approach with other carrier phase estimation methods, e.g., the RF-pilot aided algorithms [14], [15].

Based on this operation principle, a carrier recovery algorithm is designed, with its flow chart shown in Fig. 3. The received microwave signal is denoted as  $\tilde{s}$ . To reduce the computational time, only a segment of  $\tilde{s}$  is used in step 1. The signal segment is mixed with a digital carrier at the frequency of  $f_c$ . The default value of  $f_c$  is set to  $f_{c, default}$ . The output signal of the mixer is filtered by an LPF denoted by LPF 1 to remove the sum frequency image generated by the mixing process, as well as to increase the CSPR of the microwave signal by suppressing the carried data. The filtered signal is then down-sampled. The down-sampling is only performed when  $f_o$  decreases by several orders of magnitude, rather than in each iteration. Subsequently, the CPM process is carried out to search for two adjacent crossing points, with their indices denoted by  $p_1$  and  $p_2$ . To further alleviate the interference of the carried data, a periodicity test is executed to determine whether  $p_1$  and  $p_2$  are effective. If they are effective, the estimated CFO magnitude  $|f_o|$  is given by  $F_s/(2N|p_1 - p_2|)$ . Otherwise, the algorithm searches for another two crossing points, and the periodicity test is executed again. The magnitude of  $f_o$  is sent to the CFO sign recognition and step-size control modules to update  $f_o$ . Finally,  $f_c$  is updated and delivered to the next iteration. To end the iterations and start step 2, the estimated magnitude of  $f_o$  needs to be less than a threshold  $f_{o, threshold}$ . In step 2, the received microwave signal  $\tilde{s}$  is down-converted by mixing it with a digital carrier at  $f_c$ . LPF 2 is used to remove the sum frequency image without affecting the carried data. The filtered signal is down-sampled, and then its envelope is detected to obtain the residual CFO and the carrier phase. By the two steps, the carrier frequency and phase can be accurately estimated. The recovered baseband signal is sent to the demodulation module.

The detailed implementations of the CPM, CFO sign recognition and envelope detection modules are provided in the Appendix.

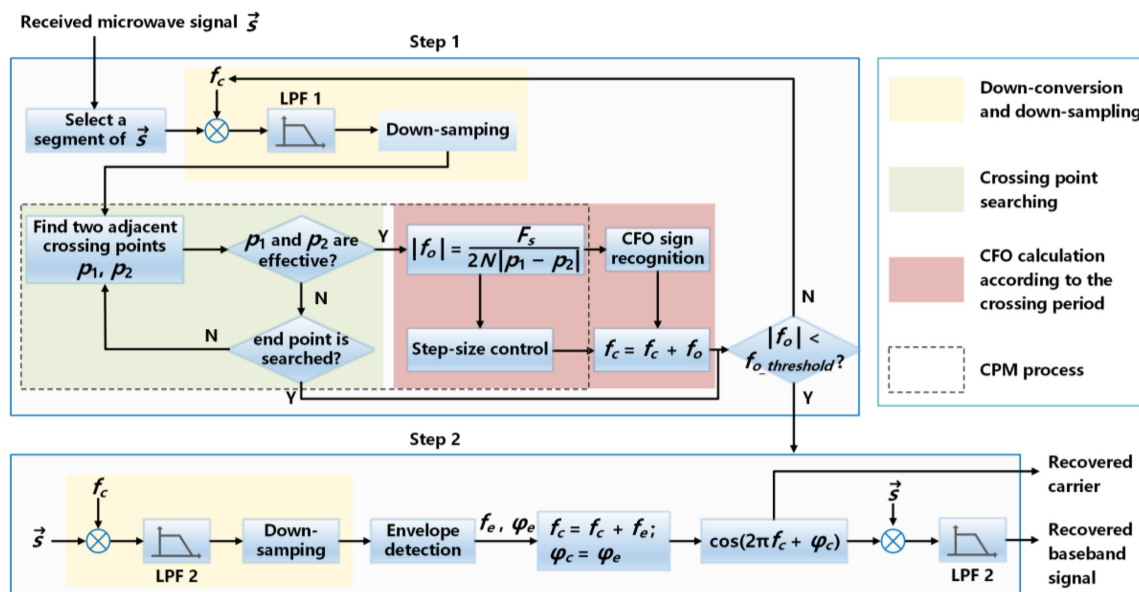


Fig. 3. Flow chart of the carrier recovery algorithm.  $N$ : down-sampling factor.  $f_o$ : estimated residual CFO.

### 3. Experimental Verifications and Discussions

A proof-of-concept experiment is performed to validate the feasibility of the proposed approach. The experimental setup is presented in Fig. 4(a). Two continuous wave (CW) lights from two free-running distributed-feedback (DFB) fiber laser sources (Koheras BASIK C15) are used as the optical carriers of the signal light and the LO light. The linewidths of the two laser sources are 5 KHz. The corresponding phase noises are less than  $5 \mu\text{rad}/\sqrt{\text{Hz/m}}$  at 1 KHz. In the experiment, the wavelength of the signal light is tuned from 1550.408 nm to 1550.168 nm with a tuning step of 8 pm, while that of the LO light is fixed at 1550.120 nm. Hence, there are 31 wavelength spacing settings from 288 pm to 48 pm. Due to a reference wavelength difference between the two laser sources of  $\sim 1$  GHz, the actual frequency spacing between the two lights varies from 37 GHz to 7 GHz. The signal light is then launched into a dual-drive Mach-Zehnder modulator (DDMZM) (T.DKH1.5-40PD-ADC). The modulator is biased at the quadrature point to preserve the optical carrier, which leads to a lower receiver sensitivity than that of optical carrier suppression (OCS) modulation for phase-modulated signals, e.g., a QPSK signal. A 2-Gbaud baseband signal with OOK/QPSK modulation format is generated by a 25-GHz arbitrary waveform generator (AWG) (Keysight M8195A). The signal is then amplified and fed into the modulator for electrical-to-optical conversion. The CSPR of the modulated signal light is set to  $\sim 8$  dB by adjusting the baseband signal amplitude in the AWG, which is also the required minimum CSPR to ensure effective carrier recovery. The signal light is launched into a 40-km single mode fiber. After the transmission, the signal light is amplified, filtered and combined with the LO light by a 50:50 optical coupler. Subsequently, the combined light is split into two parts using another 50:50 optical coupler. One part is fed into a 40-GHz photodetector (XPDV2120R) for heterodyne detection, whereas the other part is monitored by an optical spectrum analyzer (OSA) (APEX 2040C). The generated microwave signal is received by a 36-GHz digital storage oscilloscope (DSO) (LeCroy 10-36Zi-A), with a sampling rate of 80 GSa/s and a frame duration of 10  $\mu\text{s}$ . After carrier recovery and demodulation, which are implemented offline by Matlab, the baseband data can be precisely retrieved. Fig. 4(b) shows an example of the monitored optical spectrum, in which the two optical carriers are spaced by 28 GHz, and the corresponding electrical spectrum is provided in Fig. 4(c). The frequency response of the transmission system

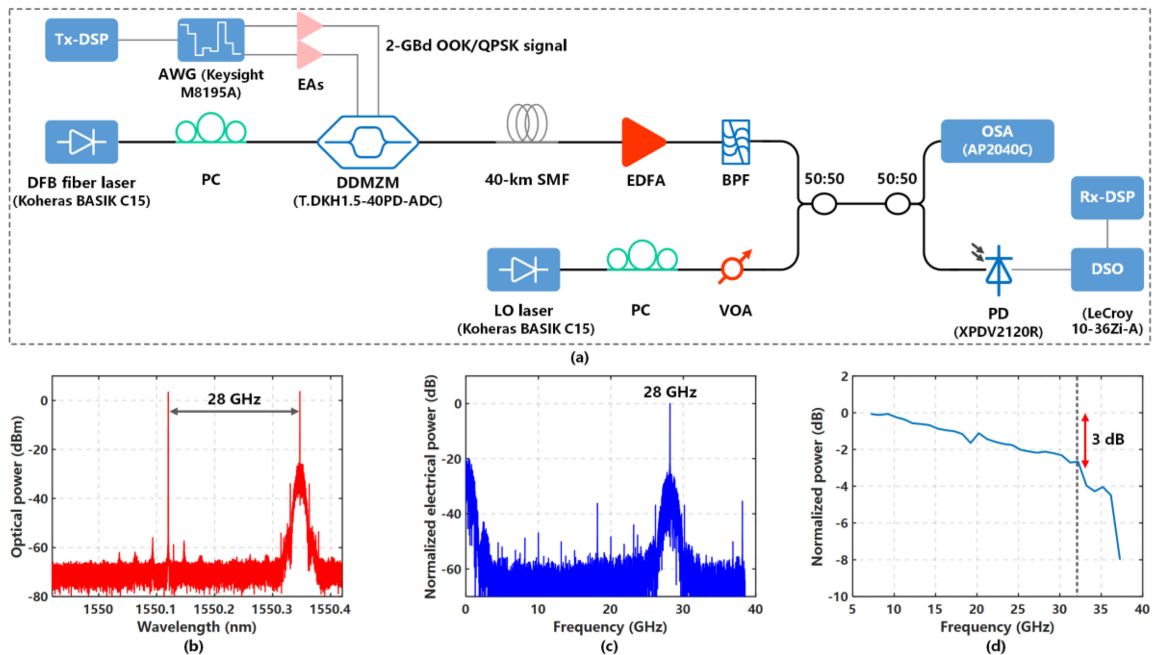


Fig. 4. (a) Experimental setup. (b) Monitored optical spectrum. (c) Normalized electrical spectrum. (d) Frequency response of the transmission system. DFB: distributed feedback. DDMZM: dual-drive Mach–Zehnder modulator. AWG: arbitrary waveform generator. SMF: single-mode fiber. EDFA: erbium-doped fiber amplifier. BPF: bandpass filter. VOA: variable optical attenuator. OSA: optical spectrum analyzer. DSO: digital storage oscilloscope.

is shown in Fig. 4(d). The response is measured by calculating the carrier power of the received microwave signal for each wavelength spacing in the DSP.

The parameters of the carrier recovery algorithm are given as follows. The default carrier frequency  $f_{c, default}$  is set to 28 GHz. The CFO threshold  $f_{o, threshold}$  is 2.2 MHz. With a frame duration of  $10 \mu\text{s}$ , each received frame contains  $8 \times 10^5$  samples ( $80 \text{ Gsa/s} \times 10 \mu\text{s}$ ). In step 1, 1000 consecutive samples are firstly used for CFO estimation without down-sampling. When the estimated crossing period is longer than the duration of the 1000 samples,  $10^5$  consecutive samples are down-sampled by a factor of 100. After coarse recovery, down-sampling of all the  $8 \times 10^5$  samples is performed with a factor of 800. Therefore, in each CPM process and the envelope detection process, only 0.125% ( $1000 / 8 \times 10^5$ ) samples are used, leading to a significantly reduced computational complexity. For the LPFs, we define the cut-off frequency as the frequency at which the signal attenuation is 30 dB. The cut-off frequency of LPF 1 varies from 20 GHz to 0.1 GHz in the CPM iterations, while that of LPF 2 is fixed at 12 GHz. Both LPF 1 and LPF 2 are digital Butterworth filters.

The proposed approach is demonstrated for a microwave signal carrying a baseband signal with OOK/QPSK modulation format for back-to-back (BTB) and fiber transmission over a single mode fiber of 40 km. Hence, there are four data groups, denoted by OOK-BTB, OOK-40 km, QPSK-BTB, and QPSK-40 km. For each data group, the wavelength tuning process of the signal light is repeated. For all the 31 wavelength spacings in each data group, carrier recovery of the received microwave signal is realized by the proposed approach. In Fig. 5, we plot the normalized waveforms of the received microwave signal, the data after coarse recovery and that after fine recovery, with the carrier frequencies of 7 GHz, 12 GHz, 17 GHz, 22 GHz, 27 GHz, 32 GHz, and 37 GHz. Note that the received signal is composed of an unused baseband component and the microwave component. The microwave signal waveforms in Fig. 5 are obtained by applying high-pass filtering to the received signal. The stopband of the filter is 0 – 6 GHz. It can be observed that, in each measurement, the microwave signal is down-converted from an AC coupled signal

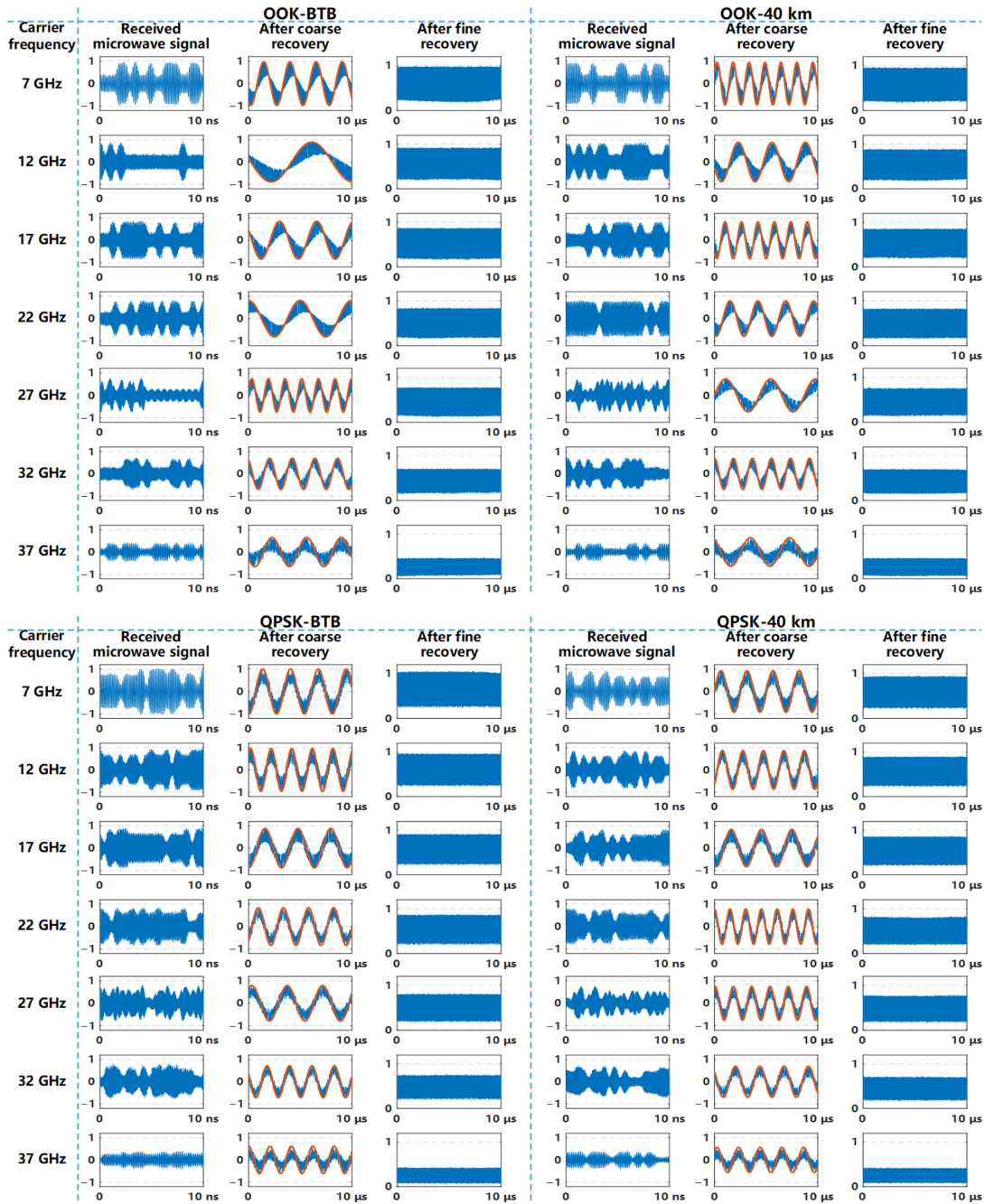


Fig. 5. Part of the normalized waveforms of the received microwave signal, the data after coarse recovery and that after fine recovery. The orange lines are the signal envelopes fitted by fine recovery.

to a DC coupled signal by the two-step carrier recovery. This means that, the CFO estimation is realized over a range of 30 GHz, and the CFO estimation errors are well below 0.1 MHz if the frame duration is 10  $\mu$ s. The wavelength-drifting of the lasers is typically at a very low speed (e.g., 100 MHz over several hours) [21], [44], so the carrier recovery algorithm experiences negligible CFO drift within the frame duration of 10  $\mu$ s. For long-term CFO estimation, the proposed algorithm can be periodically performed to track the drift.

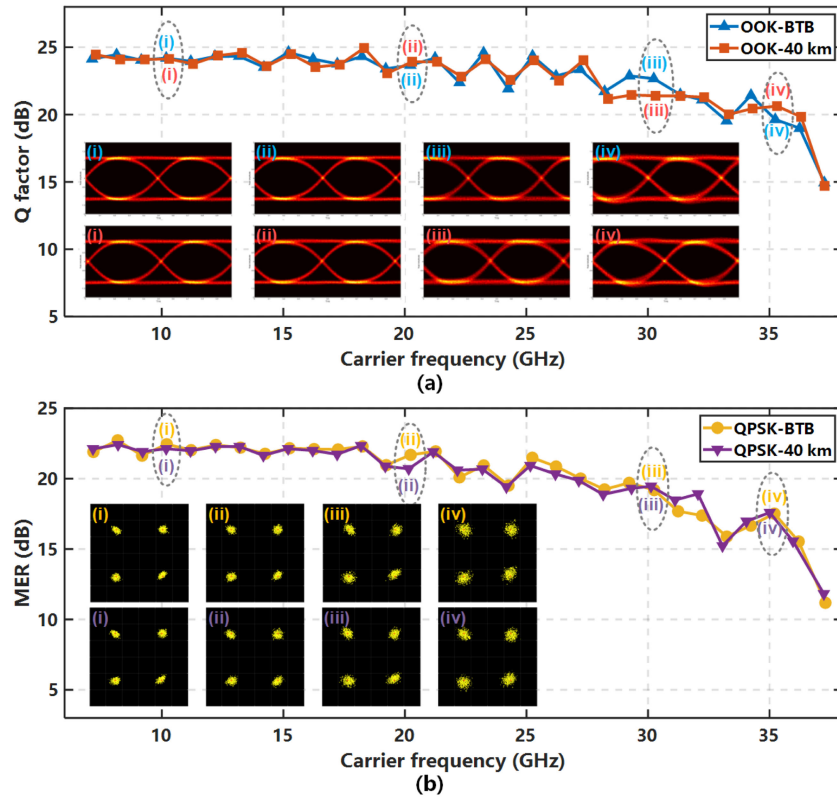


Fig. 6. (a) Q factors and demodulated eye diagrams of the recovered OOK signal. (b) MERs and demodulated constellation diagrams of the recovered QPSK signal.

The recovered baseband signal is subsequently demodulated. Fig. 6(a) shows the Q factors and the demodulated eye diagrams of the OOK signal, while the modulation error ratios (MERs) and the demodulated constellation diagrams of the QPSK signal are shown in Fig. 6(b). The Q factors and MERs are calculated by the following equations [45], [46], respectively:

$$\text{Q factor (dB)} = 20 \log_{10} \left( \frac{|\mu_1 - \mu_0|}{\sigma_1 + \sigma_0} \right), \quad (1)$$

$$\text{MER} = 10 \log_{10} \left( \frac{\sum_{n=1}^K (I_{\text{ref}}^2 + Q_{\text{ref}}^2)}{\sum_{n=1}^K ((I_{\text{ref}} - I)^2 + (Q_{\text{ref}} - Q)^2)} \right). \quad (2)$$

In Eq. (1),  $\mu_i$  and  $\sigma_i$  represent the mean value and standard deviation of the eye level  $i$  ( $i = 0, 1$ ), respectively. In Eq. (2),  $K$  is the number of symbols,  $I_{\text{ref}}/Q_{\text{ref}}$  and  $I/Q$  are the real/imaginary parts of the  $n$ -th ideal QPSK symbol and the  $n$ -th received QPSK symbol, respectively. In Fig. 6, the Q factor and MER penalties are mainly induced by the roll-off at high frequencies, as well as the polarization state and bias voltage drifts.

Fig. 7(a) shows the iteration numbers of the CPM processes for estimating different CFOs. Each data point in the figure is the result of a single measurement. For each data group, the iteration number varies from 5 to 8 with the increase of the CFO magnitude. Considering the experimental uncertainties, the measurements at CFO = 0.2 GHz and CFO = 9.3 GHz are repeated 50 times for the OOK-40 km group. The iteration numbers are shown in Fig. 7(b). The average value and the standard deviation of the iteration numbers are 5.0 and 0.2 in the measurements at CFO = 0.2 GHz, while that in the other measurements are 7.4 and 0.6.

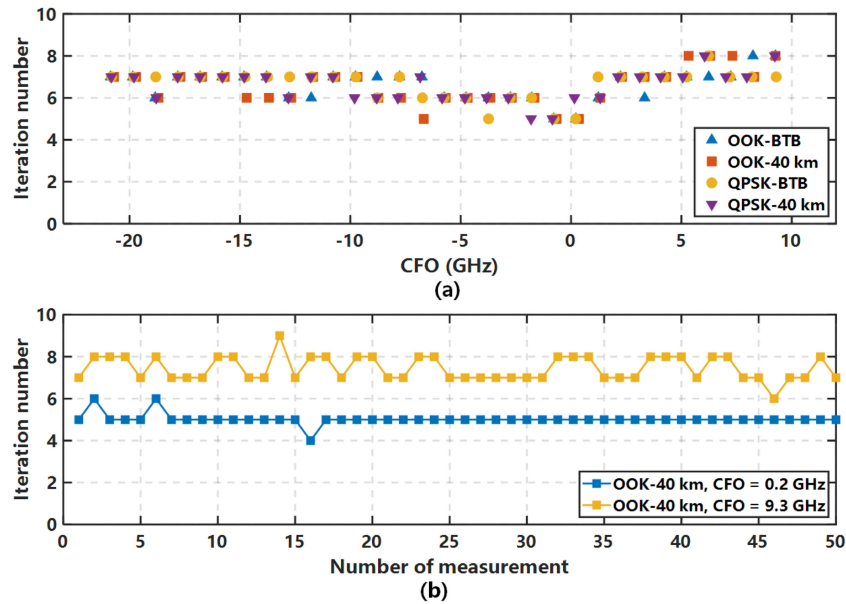


Fig. 7. Iteration numbers of the CPM processes (a) for estimating different CFOs. (b) for CFO = 0.2 GHz and CFO = 9.3 GHz in 50 measurements.

Here we provide the computational complexity of our proposed carrier recovery algorithm. The number of required real-valued multiplications is used to characterize the complexity. The total number of real-valued multiplications is  $11.1L$ , and  $\sim 9.8\%$  and  $\sim 90.2\%$  multiplications are used for the down-conversions in coarse recovery and fine recovery, respectively.  $L$  is the number of signal samples required by the algorithm. Only  $< 0.003\%$  multiplications are used for the CPM processes and the envelope detection process. Here, we provide the detailed calculation of the number of multiplications for the down-conversion in the fine recovery as an example, since the computational complexity mainly comes from this process. The input signal of the down-converter contains  $L$  samples. Firstly,  $L$  multiplications are performed in the mixing process. LPF 2 is a 5th-order infinite impulse response (IIR) filter with 9 filter coefficients, hence  $9L$  multiplications are required. The total number of multiplications in the down-conversion process is therefore  $10L$ . Similarly,  $0.13L$  and  $0.96L$  multiplications are required by the mixer and LPF 1 in the coarse recovery. The computational complexity of our algorithm increases linearly with  $L$ , and it can be further reduced through low-complexity digital down-converters. Such a down-converter may be realized by using an additional down-sampling operation before the down-conversion. Note that the computational complexity of the proposed approach is independent of the modulation format.

The proposed carrier recovery approach may also be used in a coherent optical system or a microwave photonic system employing an analog radio receiver. To achieve this,  $f_{c\_default}$  needs to be set to a proper value. The received microwave signal in the analog radio receiver is firstly down-converted to an intermediate frequency before the analog-to-digital conversion, therefore  $f_{c\_default}$  is the intermediate frequency. As for the coherent optical system,  $f_{c\_default}$  is zero since homodyne detection is employed.

The performance comparisons of various carrier recovery methods are provided in Table 1. Our proposed approach can recover both the carrier frequency in a wide range and the carrier phase, while the other methods are typically used for frequency recovery or phase recovery. The theoretical CFO estimation ranges of the BPS algorithm, the FFT-based algorithm, and the proposed method can be as large as  $\pm F_s/2$ , which are much higher than the other methods and independent of the symbol rate  $R_s$ . The available modulation formats of the  $M$ -th power algorithm are limited to  $M$ -PSK, while the other methods can be used for any modulation format of the baseband signal.

TABLE 1  
Comparison of Carrier Recovery Methods

Carrier recovery methods	CFO estimation range	CFO estimation error	Linewidth tolerance (MHz)	Modulation format of the baseband signal	Computational complexity
$M$ -th power algorithm [47], [48]	$\pm R_s/M$	$\leq 0.125R_s$	–	$M$ -PSK	$4L \times \log_2(M)$
PLL [49]	–	–	8	Any format	–
RF-pilot aided algorithm [50]	–	–	5	Any format	$(N_f + 1) \times L$
BFS algorithm [21]	$\pm F_s/2$	$\leq 3\Delta f_{\text{fine}}$ at $L = 128$	0.1	Any format	$(N_{\text{coarse}} + N_{\text{fine}}) \times T_{\text{phase}}(L)$
FFT-based algorithm [24]	$\pm F_s/2$	$\leq F_s / (2L)$	–	Any format	$2L \times \log_2(L)$
Training sequence-based algorithm [31]	$\pm R_s/2$	$\leq 0.29R_s / L$	1	Any format	$2L$
This work	$\pm F_s/2$	well below $F_s/L$	0.005	Any format	$11.1L$

$M$ : number of constellation points.  $R_s$ : symbol rate.  $L$ : number of signal samples used for recovery.  $N_f$ : number of filter coefficients of a band-pass filter.  $F_s$ : sampling frequency.  $\Delta f_{\text{fine}}$ : step size in fine recovery.  $N_{\text{coarse}}/N_{\text{fine}}$ : number of searching steps in the coarse/fine recovery.  $T_{\text{phase}}(L)$ : number of real-valued multiplications required for phase recovery of  $L$  samples. –: not specified.

The computational complexity of our method is higher than the training sequence-based algorithm, but it is significantly lower than the BFS and FFT-based algorithms since the values of  $L$  in the three methods need to be large enough to achieve relatively small CFO estimation errors (e.g., several MHz for the sampling frequency at tens of GHz).

## 4. Conclusion

We proposed and demonstrated an approach to implement carrier frequency and phase recovery of a microwave photonic signal. By using the CPM, CFO sign recognition and envelope detection modules, wideband and high accuracy carrier recovery of a microwave photonic signal was achieved. A proof-of-concept experiment was performed in a microwave photonic system employing optical heterodyne detection. In the experiment, a microwave signal carrying OOK/QPSK data was generated and detected for BTB and for fiber transmission over a 40-km single mode fiber. In all the measurements, the carrier frequency and phase recovery were realized. The CFO estimation range was from  $-21$  GHz to  $+9$  GHz, and the CFO estimation errors were less than 0.1 MHz for a frame duration of  $10 \mu\text{s}$ .

## Appendix Flow Chart of Carrier Period Measurement

Fig. 8 depicts the detailed flow chart of the CPM process. The down-sampled microwave signal is denoted as  $\vec{d}$ .  $d(k)$  represents the  $k$ -th point in  $\vec{d}$ . A feedback loop is used to search for  $p_1$  and  $p_2$  point by point. In the loop, if the sign of  $d(k)$  differs from that of  $d(k-1)$ , a crossing point must exist between  $k$  and  $k-1$ . Its index  $p_1/p_2$  is then calculated by a linear function shown in Fig. 8. If  $p_1$  and  $p_2$  are found, their midpoint and time difference are calculated and denoted as  $p_0$  and  $span$ , respectively. In the periodicity test, there are two cases in which  $p_1$  and  $p_2$  are effective:

- 1) Calculate the signs of five points  $[d_0, d_1, d_2, d_3, d_4]$ , which are given by  $d_i = d(p_0 + span \times i)$ . The signs alternate between positive and negative values, i.e.,  $[+, -, +, -, +]$  or  $[-, +, -, +, -]$ ;

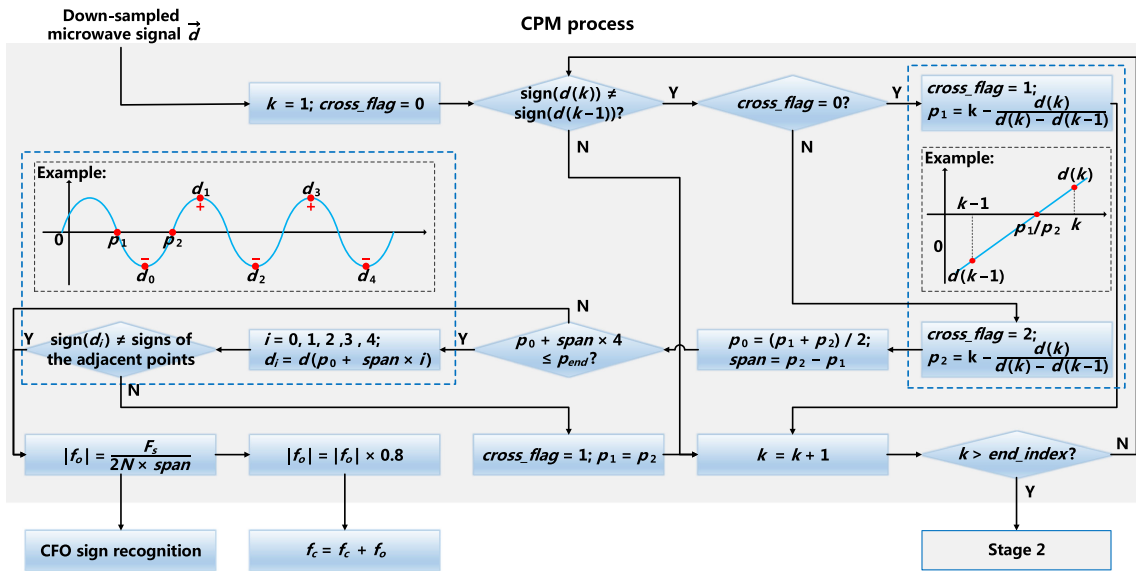


Fig. 8. Detailed flow chart of the CPM process.  $\text{sign}(\cdot)$  is a function that extracts the sign of the input variable.  $N$ : down-sampling factor.

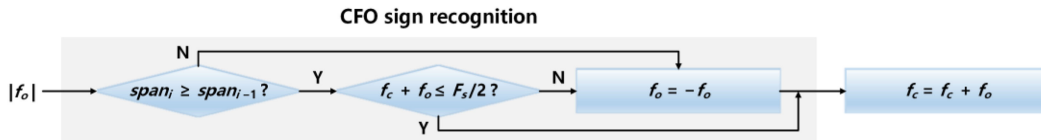


Fig. 9. Detailed flow chart of the CFO sign recognition process.

2)  $span$  is large enough such that  $p_0 + span \times 4 > p_{\text{end}}$  is satisfied, where  $p_{\text{end}}$  is the index of the end point.

Once both  $p_1$  and  $p_2$  are effective, the magnitude of  $f_o$  is calculated and slightly reduced. This reduction is required, because the sign of  $f_o$  in the next iteration is uncertain if the estimated magnitude of  $f_o$  in this iteration is too accurate. With the deviation, the sign of  $f_o$  remains unchanged in the following iterations. After the step-size control of  $f_o$ ,  $f_c$  is updated accordingly. If  $p_1$  or  $p_2$  is not effective, the value of  $p_2$  is assigned to  $p_1$ , and the algorithm searches for effective  $p_2$  again.

*Flow Chart of CFO Sign Recognition:* The CFO sign recognition operation was proposed for fast Fourier transform (FFT) based carrier recovery algorithms [21]. Based on the same principle, here we provide its implementation in our CPM-based carrier recovery approach. As shown in Fig. 9,  $span_i$  represents the  $span$  in the  $i$ -th CPM iteration. In the first iteration,  $f_o$  can be set to either positive or negative. In the following iterations, if  $span_i \geq span_{i-1}$  and  $f_c + f_o \leq F_s/2$  are satisfied, the sign of  $f_o$  remains unchanged. Otherwise, the sign is inverted. Also, if the sign of the actual CFO changes in an iteration, an additional CPM iteration is required to correct the sign of the estimated CFO.

*Flow Chart of Envelope Detection:* The fine CFO estimation and the phase estimation are realized by a feedforward envelope detection method. Fig. 10 shows the detailed flow chart. The magnitude of the input signal is extracted and expressed as  $|\vec{d}'|$ . The envelope of  $|\vec{d}'|$  is periodic, with the period denoted as  $T_e$ . Then,  $|\vec{d}'|$  is divided into multiple segments by serial-to-parallel conversion, and the maximum of each segment is calculated. Then, the maxima above an amplitude threshold are selected and combined to form a new signal  $\vec{m}$ . The angle of  $\vec{m}$  is then obtained through the arccosine function and denoted as  $\vec{m}'$ . Due to the periodicity of the envelope,  $\vec{m}'$  requires phase

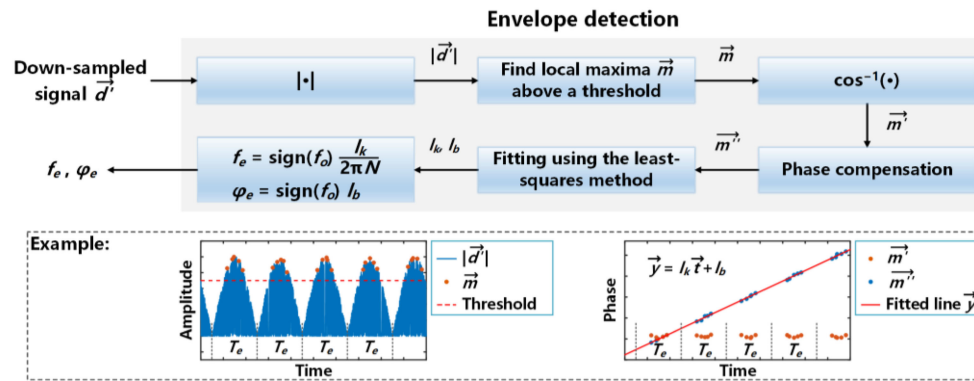


Fig. 10. Detailed flow chart of the envelope detection process.  $|\cdot|$  is a function that calculates the absolute value of the input variable.  $\bar{t}$  represents the time.

compensation to be linearly dependent on time. To achieve this, the sign of the  $i$ -th point  $m'(i)$  is inverted if  $m'(i)$  is greater than  $m'(i+1)$  and they are in the same period  $T_e$ , and a phase of  $(k-1)\pi$  radians is added to all the points in the  $k$ -th period. The phase-compensated signal, denoted as  $\vec{m}'$ , is roughly linearly dependent on time.  $\vec{m}'$  is then fitted by the least-squares method. The slope  $l_k$  and y-intercept  $l_b$  of the fitted linear curve  $\vec{y}$  are used to calculate the frequency  $f_e$  and phase  $\varphi_e$  of the envelope, which are also the residual CFO and the carrier phase, respectively.

## References

- [1] J. Capmany and D. Novak, "Microwave photonics combines two worlds," *Nature Photon.*, vol. 1, no. 6, pp. 319–330, 2007.
- [2] J. Yao, "Microwave photonics," *J. Lightw. Technol.*, vol. 27, no. 3, pp. 314–335, Feb. 2009.
- [3] U. Gliese, T. N. Nielsen, S. Norskov, and K. E. Stubkjaer, "Multifunctional fiber-optic microwave links based on remote heterodyne detection," *IEEE Trans. Microw. Theory Techn.*, vol. 46, no. 5, pp. 458–468, May 1998.
- [4] R. Cao *et al.*, "Integrated multi-channel millimeter wave photonic generation based on a silicon chip with automated polarization control," in *Proc. Eur. Conf. Opt. Commun.*, 2018, Paper We2.43.
- [5] L. Zhang, X. Hu, P. Cao, Q. Chang, and Y. Su, "Simultaneous generation of independent wired and 60-GHz wireless signals in an integrated WDM-PON-RoF system based on frequency-sexupling and OCS-DPSK modulation," *Opt. Exp.*, vol. 20, no. 13, pp. 14648–14655, 2012.
- [6] J. Wu *et al.*, "Passive silicon photonic devices for microwave photonic signal processing," *Opt. Commun.*, vol. 373, pp. 44–52, 2016.
- [7] J. Zhang, J. Yu, N. Chi, Z. Dong, X. Li, and G. K. Chang, "Multichannel 120-Gb/s data transmission over  $2 \times 2$  MIMO fiber-wireless link at W-band," *IEEE Photon. Technol. Lett.*, vol. 25, no. 8, pp. 780–783, Apr. 2013.
- [8] X. Li *et al.*, "120Gb/s wireless Terahertz-wave signal delivery by 375GHz-500GHz multi-carrier in a  $2 \times 2$  MIMO system," in *Proc. Opt. Fiber Commun. Conf.*, 2018, Paper M4J.4.
- [9] L. Tao *et al.*, "Experimental demonstration of 48-Gb/s PDM-QPSK radio-over-fiber system over 40-GHz mm-wave MIMO wireless transmission," *IEEE Photon. Technol. Lett.*, vol. 24, no. 24, pp. 2276–2279, Dec. 2012.
- [10] D. Zibar *et al.*, "High-capacity wireless signal generation and demodulation in 75-to 110-GHz band employing all-optical OFDM," *IEEE Photon. Technol. Lett.*, vol. 23, no. 12, pp. 810–812, Jun. 2011.
- [11] R. Puerta, J. Yu, X. Li, Y. Xu, J. J. V. Olmos, and I. T. Monroy, "Demonstration of 352 Gbit/s photonically-enabled D-band wireless delivery in one  $2 \times 2$  MIMO system," in *Proc. Opt. Fiber Commun. Conf.*, 2017, Paper Tu3B.3.
- [12] M. Nakazawa, J. Hongo, K. Kasai, and M. Yoshida, "Polarization-multiplexed 1 Gsymbol/s, 64 QAM (12 Gbit/s) coherent optical transmission over 150 km with an optical bandwidth of 2 GHz," in *Proc. Opt. Fiber Commun. Conf.*, 2007, Paper PDP26.
- [13] W. R. Peng, T. Tsuritani, and I. Morita, "Simple carrier recovery approach for RF-pilot-assisted PDM-CO-OFDM systems," *J. Lightw. Technol.*, vol. 31, no. 15, pp. 2555–2564, Aug. 2013.
- [14] S. L. Jansen, I. Morita, T. C. W. Schenk, N. Takeda, and H. Tanaka, "Coherent optical 25.8-Gb/s OFDM transmission over 4160-km SSMAF," *J. Lightw. Technol.*, vol. 26, no. 1-4, pp. 6–15, Jan. 2008.
- [15] H. Tanaka, I. Morita, N. Takeda, and S. L. Jansen, "20-Gb/s OFDM transmission over 4,160-km SSMF enabled by RF-pilot tone phase noise compensation," in *Proc. Opt. Fiber Commun. Conf.*, 2007, Paper PDP15.
- [16] Y. Shoji, K. Hamaguchi, and H. Ogawa, "Millimeter-wave remote self-heterodyne system for extremely stable and low-cost broad-band signal transmission," *IEEE Trans. Microw. Theory Techn.*, vol. 50, no. 6, pp. 1458–1468, Jun. 2002.

- [17] S. Liu, P. C. Peng, M. Xu, D. Guidotti, H. Tian, and G. K. Chang, "A long-distance millimeter-wave RoF system with a low-cost directly modulated laser," *IEEE Photon. Technol. Lett.*, vol. 30, no. 15, pp. 1396–1399, Aug. 2018.
- [18] X. Li and J. Yu, "Generation and heterodyne detection of >100-Gb/s Q-band PDM-64QAM mm-wave signal," *IEEE Photon. Technol. Lett.*, vol. 29, no. 1, pp. 27–30, Jan. 2017.
- [19] N. G. Gonzalez, D. Zibar, A. Caballero, and I. T. Monroy, "Experimental 2.5-Gb/s QPSK WDM phase-modulated radio-over-fiber link with digital demodulation by a K-means algorithm," *IEEE Photon. Technol. Lett.*, vol. 22, no. 5, pp. 335–337, Mar. 2010.
- [20] N. K. Mallat and S. O. Tatu, "Carrier recovery loop for millimeter-wave heterodyne receiver," in *Proc. Biennial Symp. Commun.*, 2008, pp. 239–242.
- [21] X. Zhou, "Efficient clock and carrier recovery algorithms for single-carrier coherent optical systems: A systematic review on challenges and recent progress," *IEEE Signal Process. Mag.*, vol. 31, no. 2, pp. 35–45, Mar. 2014.
- [22] T. Nakagawa *et al.*, "Wide-range and fast-tracking frequency offset estimator for optical coherent receivers," in *Proc. Eur. Conf. Opt. Commun.*, 2010, Paper We7A.2.
- [23] W. Shieh and W. Chen, "Optical carrier recovery using feedforward phase compensation," in *Proc. Eur. Conf. Opt. Commun.*, 2004, pp. 654–655.
- [24] X. Zhou, X. Yang, R. Li, and K. Long, "Efficient joint carrier frequency offset and phase noise compensation scheme for high-speed coherent optical OFDM systems," *J. Lightw. Technol.*, vol. 31, no. 11, pp. 1755–1761, Jun. 2013.
- [25] Z. Liu, D. S. Wu, D. J. Richardson, and R. Slavik, "Homodyne OFDM using simple optical carrier recovery," in *Proc. Opt. Fiber Commun. Conf.*, 2014, Paper W4K.3.
- [26] X. Zhou *et al.*, "64-Tb/s, 8 b/s/Hz, PDM-36QAM transmission over 320 km using both pre- and post-transmission digital signal processing," *J. Lightw. Technol.*, vol. 29, no. 4, pp. 571–577, Feb. 2011.
- [27] X. Zhou, "Hardware efficient carrier recovery algorithms for single-carrier QAM systems," in *Proc. Adv. Photon. Congr.*, 2012, Paper SpTu3A.1.
- [28] S. Dris, I. Lazarou, P. Bakopoulos, and H. Avramopoulos, "Phase entropy-based frequency offset estimation for coherent optical QAM systems," in *Proc. Opt. Fiber Commun. Conf.*, 2012, Paper OTu2G.4.
- [29] T. Nakagawa, T. Kobayashi, K. Ishihara, and Y. Miyamoto, "Wide-range and fast-tracking non-data-aided frequency offset estimator for QAM optical coherent receivers," *IEICE Trans. Commun.*, vol. E99b, no. 7, pp. 1416–1425, 2016.
- [30] X. Zhou *et al.*, "High spectral efficiency 400 Gb/s transmission using PDM time-domain hybrid 32-64 QAM and training-assisted carrier recovery," *J. Lightw. Technol.*, vol. 31, no. 7, pp. 999–1005, Apr. 2013.
- [31] X. Zhou, X. Chen, and K. Long, "Wide-range frequency offset estimation algorithm for optical coherent systems using training sequence," *IEEE Photon. Technol. Lett.*, vol. 24, no. 1, pp. 82–84, Jan. 2012.
- [32] R. Koma, M. Fujiwara, R. Igarashi, T. Kanai, J. Kani, and A. Otaka, "Wide range carrier frequency offset estimation method using training symbols with asymmetric constellations for burst-mode coherent reception," in *Proc. Opt. Fiber Commun. Conf.*, 2018, Paper M3B.5.
- [33] A. Spalvieri and L. Barletta, "Pilot-aided carrier recovery in the presence of phase noise," *IEEE Trans. Commun.*, vol. 59, no. 7, pp. 1966–1974, Jul. 2011.
- [34] W. Y. Kuo and M. P. Fitz, "Frequency offset compensation of pilot symbol assisted modulation in frequency flat fading," *IEEE Trans. Commun.*, vol. 45, no. 11, pp. 1412–1416, Nov. 1997.
- [35] Y. Yang *et al.*, "Fast, accurate, and robust frequency offset estimation based on modified adaptive Kalman filter in coherent optical communication system," *Opt. Eng.*, vol. 56, no. 9, pp. 096109, 2017.
- [36] L. Li, Z. Tao, S. Oda, T. Hoshida, and J. C. Rasmussen, "Wide-range, accurate and simple digital frequency offset compensator for optical coherent receivers," in *Proc. Opt. Fiber Commun. Conf.*, 2008, Paper OWT4.
- [37] Z. Tao and H. Zhang, "Simple, robust, and wide-range frequency offset monitor for automatic frequency control in digital coherent receivers," in *Proc. Eur. Conf. Opt. Commun.*, 2007, Paper 3.5.
- [38] A. A. Abidi, "The path to the software-defined radio receiver," *IEEE J. Solid-State Circuits*, vol. 42, no. 5, pp. 954–966, May 2007.
- [39] N. C. Davies, "A high performance HF software radio," in *Proc. Intl. Conf. HF Radio Syst. Techn.*, 2000, pp. 249–256.
- [40] X. Li *et al.*, "Delivery of 54-Gb/s 8QAM W-band signal and 32-Gb/s 16QAM K-band signal over 20-km SMF-28 and 2500-m wireless distance," *J. Lightw. Technol.*, vol. 36, no. 1, pp. 50–56, Jan. 2018.
- [41] S. Kowlgi, P. Mattheijssen, C. Berland, and T. Ridgers, "EVM considerations for convergent multi-standard cellular base-station transmitters," in *Proc. IEEE Int. Symp. Personal, Indoor Mobile Radio Commun.*, 2011, pp. 1865–1869.
- [42] M. Grigat, *Phase Noise Aspects, Project: IEEE P802.15 Working Group for Wireless Personal Area Networks (WPANs)*, IEEE P802.15, 2013.
- [43] Y. Zhao *et al.*, "100-Hz linewidth diode laser with external optical feedback," *IEEE Photon. Technol. Lett.*, vol. 24, no. 20, pp. 1795–1798, Oct. 2012.
- [44] F. Späth, S. Metzendorf, A. Behrendt, H. D. Wizemann, G. Wagner, and V. Wulfmeyer, "Online/offline injection seeding system with high frequency-stability and low crosstalk for water vapor DIAL," *Opt. Commun.*, vol. 309, pp. 37–43, 2013.
- [45] N. S. Bergano, F. W. Kerfoot, and C. R. Davidson, "Margin measurements in optical amplifier system," *IEEE Photon. Technol. Lett.*, vol. 5, no. 3, pp. 304–306, Mar. 1993.
- [46] "ETR 290: Measurement guidelines for DVB systems," ETSI Tech. Rep., Sophia Antipolis CEDEX, France, Tech. Rep. ETR 290, 1997.
- [47] A. J. Viterbi and A. M. Viterbi, "Nonlinear estimation of PSK-modulated carrier phase with application to burst digital transmission," *IEEE Trans. Inf. Theory*, vol. IT-29, no. 4, pp. 543–551, Jul. 1983.
- [48] Y. Jiang, R. L. Richmond, and J. S. Baras, "Carrier frequency estimation of MPSK modulated signals," Univ. Maryland, College Park, MD, USA, Tech. Res. Rep. CSHCN T.R. 99-3, 1999.
- [49] U. Giliese *et al.*, "A wideband heterodyne optical phase-locked loop for generation of 3-18 GHz microwave carriers," *IEEE Photon. Technol. Lett.*, vol. 4, no. 8, pp. 936–938, Sep. 1992.
- [50] S. L. Jansen, I. Morita, and H. Tanaka, "10-Gb/s OFDM with conventional DFB lasers," in *Proc. Eur. Conf. Opt. Commun.*, 2007, Paper Tu.25.2.